American Mineralogist, Volume 88, pages 1091–1103, 2003

Partitioning of Sr, Ba, Rb, Y, and LREE between plagioclase and peraluminous silicic magma

MINGHUA REN,* DON F. PARKER, AND JOHN C. WHITE†

Department of Geology, Baylor University, Waco, Texas 76798, U.S.A.

ABSTRACT

Trace-element partition coefficients between plagioclase and coexisting glass/matrix have been determined for twenty-nine rhyodacite-rhyolite samples from nine volcanic centers. Strontium partition coefficients form two clear positive trends when plotted against the An content of plagioclase. One trend has a steep slope with D_{Sr} between 5.6 and 15.8 (T1), whereas the other trend has a gentle slope with D_{Sr} between 1.2 and 7.6 (T2). Barium partition coefficients show similar patterns: a steeply sloped trend is formed by samples with D_{Ba} between 1.6 and 8.8, and a gently sloped trend by samples with D_{Ba} <1. D_{Sr} and D_{Ba} in plagioclase correlate positively, and both D_{Sr} and D_{Ba} correlate positively with temperature. Samples with large D_{Sr} and D_{Ba} are all from rocks with <1 wt% CaO. These rocks are peraluminous and also have low total Sr and Ba. Partition coefficients for Sr and Ba are influenced by whole-rock CaO in high-Al rhyolite systems. Where these systems have low CaO, the opportunity increases for other divalent cations to enter the plagioclase structure. Strontium and Ba will then enter the M position of plagioclase to balance the charge deficiency caused by the substitution of Al for Si. Because of the potent influence of whole-rock composition on Sr and Ba partitioning for low CaO rocks, values of partition coefficients in petrogenetic modeling needs to be selected carefully.

INTRODUCTION

Modeling of petrological processes requires information on trace-element partitioning between coexisting crystals and liquid. The relatively simple mineralogy of peraluminous rocks affords the opportunity to model their evolution using trace-element partitioning equations. Plagioclase is an important target for this study because of its relevance to many geological problems. Empirical and experimental studies of trace-element partitioning have focused on basaltic and andesitic systems (Berlin and Henderson 1969; Philpotts and Schnetzler 1970; Schnetzler and Philpotts 1970; Sun et al. 1974; Shimizu 1978; Bacon et al. 1987; Bindeman et al. 1998; Bindeman and Davis 2000; many others). These studies confirm considerable variation in partition coefficients for plagioclase (Wilson 1989). Partitioning studies for plagioclase in rhyolite, however, are relatively few (Ewart and Taylor 1969; Nagasawa and Schnetzler 1971; Hildreth 1977; Mahood and Hildreth 1983; Nash and Crecraft 1985; others).

Because partition coefficients have a complex relationship to melt composition, crystal composition, temperature, and pressure (Albarede 1975; Arth 1976; Wood and Fraser 1976; Green and Pearson 1983; Blundy and Wood 1991; Auwera et al. 2000), it is difficult to choose appropriate values to model petrogenetic problems (Leeman and Phelps 1981; Mahood and Hildreth 1983; Icenhower and London 1996). Therefore, some investigators (e.g., Leeman and Phelps 1981; Mahood and Hildreth 1983) have suggested that it is not appropriate to use partition coefficients determined from one specific suite of rocks for modeling others. To address this problem, some predictive models have been developed that emphasize the relationship between partition coefficients and intensive variables (Sun et al. 1974; Guo and Green 1989; Blundy and Wood 1991; Icenhower and London 1996; Bindeman et al. 1998; Holt 1998; Ren et al. 2000; White et al. 2000; White 2003).

A plagioclase/melt partitioning model using data from many systems has been presented by Blundy and Wood (1991). Data points for high-silica volcanic rocks in their compilation show some scatter. Our measured Sr and Ba partition coefficients also agree poorly with the values predicted by their model.

In this paper, we present data for 29 samples of peraluminous and metaluminous rhyodacite and high-silica rhyolite from several volcanic systems. The partition coefficients for Sr, Ba, Rb, Y, Zr, and LREE were determined for plagioclase. The influences of melt and plagioclase compositions on partition coefficients for Sr, Ba, Rb, Y, and LREE are discussed. New empirical regression equations describing partitioning of Sr, Ba, La, and Ce between plagioclase and peraluminous felsic magma are presented, and comparisons are made with results from previous investigations.

SAMPLE LOCATIONS AND SAMPLE PREPARATION

Rhyodacite and rhyolite samples were collected from numerous volcanic centers located mainly in the western United States. Studied areas include Thomas Range, Utah; Long Valley Caldera, California; Brothers Fault Zone, South

* Present address: Department of Geological Science, The University of Texas at El Paso, El Paso, TX 79912. E-mail: ren@geo.utep.edu
† Present address: Department of Geological, Environmental, and Marine Sciences, Elizabeth City State University, Elizabeth City, NC 27909.

0003-004X/03/0007–1091$05.00

Sister, and Crater Lake, Oregon; Valles Caldera and Taylor Creek Rhyolite, New Mexico; and one sample from Lipari, Italy. In these volcanic systems, each sample was collected from a different volcanic dome, lava flow, or, for two units, pumice from a pyroclastic deposit (Table 1).

Samples were crushed into granules with a hammer and stainless steel plate. A split of the granules was reduced to powder using a shatterbox equipped with a tungsten-carbide grinding vessel. The resultant powders were then pressed into pellets for whole-rock major- and trace- element wavelength dispersive X-ray fluorescence (WD-XRF) analysis (Appendix I[1]). Error estimates were performed by applying the method of Ragland (1989) to our XRF data according to duplicate analyses of internal standards not included in interpretation calibration. Data for duplicate analyses were from standards BBB (University of Texas at Austin), BCR-P (Washington State University), 86611B (Baylor University), and 93906 (a rhyolite sample), which are listed in Ren (1997).

Some low-Ca units contain low concentrations of Sr and Ba. To confirm the accuracy of XRF analyses for low concentration elements, selected samples also were analyzed by inductively coupled plasma-mass spectrometer (ICP-MS) at ALS-Chemex (Appendix II[1]). Strontium, Ba, and Zr agree well for both methods. Lanthanum and Ce have high correlation coefficient (r^2), but XRF data are systematically lower than ICP-MS.

Glass/matrix and feldspar plus quartz were concentrated by magnetic separation, and then handpicked under a binocular microscope. The purity of feldspar and glass is over 99%, whereas the purity of matrix is better than 95%.

For some studied units, both plagioclase and sanidine occur in the feldspar separates. Heavy liquid (sodium polytungstate) was used to separate the two feldspars. At a heavy liquid density of 2.62, all sanidine floated and plagioclase sank.

[1]For a copy of Appendices I through VI, document item AM-03-035, contact the Business Office of the Mineralogical Society of America (see inside front cover of recent issue) for price information. Deposit items may also be available on the American Mineralogist web site at http://www.minsocam.org.

Separations of 4 to 6 grams glass and plagioclase were washed thoroughly in distilled water, soaked in 10% HCl overnight, washed in deionized water again, and dehydrated by acetone.

Glass and plagioclase separates were powdered for analysis using an agate mortar. Pellets were made for WD-XRF analysis (Appendix III, IV)[1].

For samples where the mass of plagioclase was insufficient for WD-XRF analyses (less than 4 g), they were analyzed by inductively coupled plasma-atomic emission spectroscopy (ICP-AES) at Texas Tech University. Several plagioclase samples were analyzed by both WD-XRF and ICP-AES (Appendix IV). The results demonstrate strong agreement between both techniques for trace elements, except for Zr and Nb. XRF appears more reliable for low concentrations of Zr than ICP-AES.

Major-element analyses of plagioclase were performed at Baylor University using a Cameca Camebax electron microprobe. The operating conditions were 15 kV accelerating voltage and 10 nA emission current. Appropriate silicates and oxides were used as standards. The results are integrated with whole-plagioclase trace-element data (WD-XRF and ICP-AES) (Appendix IV). The reported major-element values are averages of 10–50 spots.

For systems with coexisting plagioclase and alkali feldspar, feldspar geothermometry was used to evaluate the crystallization temperature of the magma (Elkins and Grove 1990; Wen 1996) (Appendix I). For zoned plagioclase, only rim compositions were used to calculate temperatures. The Elkins and Grove (1990) model was used because it was the most recent one incorporated in the program of Wen (1996) that successfully modeled all data in our study. For three samples of the El Cajete series, Valles Caldera, both feldspar and Fe-Ti oxide compositions were used to calculate temperature, and the results are in good agreement (Ren 1997). The temperature range for studied systems was 686–878 °C (Appendix I).

PETROLOGICAL AND MINERALOGICAL CLASSIFICATION

The SiO_2 content of studied samples ranges from 68.1 to 77.3 wt%. Total $Na_2O + K_2O$ is over 8 wt%, and the samples

TABLE 1. Summary of the units studied by this investigation

Symbol	Unit	Location	Sample type	Age	SiO_2 wt%	References
Lipari	V. ne Gabellotto	Island of Lipari, Aeolian Arc, Southern Italy	Lava flow	8.6 Ka	74.8–75.1	Crisci et al. 1991
Topaz Mtn	Topaz Mountain	Thomas Range, Utah	Lava flow	6–7 Ma	74.2–76.6	Lindsey 1982; Christiansen et al. 1984
Long Valley	Glass Creek	Inyo volcanic chain, Long Valley, California	Dome	0.55–0.65 Ka	71.5–72.0	Miller 1985; Sampson and Cameron 1987
Obsidian Dome			Dome	0.55–0.65 Ka	70.0–74.0	Bailey et al. 1983; Miller 1985
	Deer Mountain	Moat-rhyolite dome, 1092 Long Valley, CA	Dome	115 Ka	71.5–72.5	Rinehart and Huber 1965
	Punch Bowl Dome	Mono volcanic chain, Long Valley, CA	Dome	5.8 Ka	76.1–77.2	Wood 1977; Sieh and Bursik 1986
Clear Lake	Thurston Creek	Hesse Flat, Clear Lake, California	Lava flow	560 Ka	74.8–75.6	Donnelly-Nolan et al. 1981; Stimac et al. 1990
Brothers FZ	Fredericks Butte	Cougar Peak, Brothers Fault Zone, Southeastern Oregon	Dome	3.90 Ma		MacLeod et al. 1976
	Elk Butte	Elk Mt., Brothers Fault Zone, Southeastern Oregon	Dome	6.67 Ma	75.7–76.2	
South Sister	Rock Mesa	South Sister, Oregon	Dome	2.56–2.74 Ka	73.3–73.6	Scott 1983; 1987; Price 1993
	Devils Hill		Lava flow	1.97–2.48 Ka	72.5–72.8	
Crater Lake	PHO, LR	Llao Rock, Crater Lake, Oregon	Lava flow	7.01 Ka	70.3–70.8	Bacon 1983; Bacon and Druitt 1988;
	PHO, CW	Cleetwood, Crater Lake, Oregon	Lava flow	6.85 Ka	70.3–70.8	Nelson et al. 1994
	PPO, RD	Redcloud Cliff, Crater Lake, Oregon	Lava flow	30 Ka	70.6–71.0	
	PPO, GH	Grouse Hill, Crater Lake, Oregon	Dome	30 Ka	70.4–71.0	
Taylor Creek	Tt11/SMC	Boiler Peak, Taylor Creek, New Mexico	Dome	24–27.7 Ma	76.9–78.9	Duffield and Dalrymple 1990
SMR	South Mountain	Valle Grande, Valles Caldera, NM	Lava flow	507–517 Ka	75.6–76.7	Spell and Kyle 1989; Spell et al. 1993
El Cajete S.	Banco Bonito	El Cajete Series, Valles Caldera, NM	Lava flow	130 Ka	73.1–75.9	Self et al. 1986; Self et al. 1988;
	Battleship Rock		Pyroclastic	59–140 Ka	73.4–74.9	Toyoda et al. 1995;
	El Cajete		flow	50–151 Ka	72.3–73.9	Ren 1997

classify as trachydacite and rhyolite (Le Bas et al. 1986). According to the aluminum saturation index [ASI = molar Al_2O_3/(Na_2O + K_2O + CaO)] and the agpaitic index [AI = (Na_2O + K_2O)/ Al_2O_3] (Appendix I), most samples are peraluminous, but samples from Crater Lake are metaluminous.

All samples are porphyritic with plagioclase phenocrysts ranging from 1 to 22 volume percent (Appendix V[1]). In more than two-thirds of the samples, plagioclase is the dominant phenocryst. Most plagioclase grains are compositionally zoned with higher An in their cores (Appendix IV).

Plagioclases from the El Cajete Series (ECS), Valles Caldera, contain an estimated 10–15% melt inclusion. The K_2O difference between bulk plagioclase and microprobe analysis was used to estimate and correct for this influence. Partition coefficients of ECS, uncorrected and corrected, are listed in Table 2.

Plagioclase-melt partition coefficients

Empirical partition coefficients were calculated by dividing the concentration of the element of interest in plagioclase and by the concentration of that element in the glass. According to the terminology presented by Beattie et al. (1993), this concentration ratio is expressed as:

$$D(\mathrm{M})^{\mathrm{Pl/gl}} = C(\mathrm{M})^{\mathrm{Pl}}/C(\mathrm{M})^{\mathrm{gl}} \quad (1)$$

where D, M, C, Pl, and gl represent the partition coefficient, the element of interest, the concentration of a component in plagioclase and glass, respectively. Calculated partition coefficients are listed in Table 2.

For systems with coexisting plagioclase and sanidine, the sanidine can concentrate some compatible trace elements, especially Ba and Sr (Berlin and Henderson 1969). In general, sanidine crystallizes later than plagioclase in rhyolitic systems (Tuttle and Bowen 1958). In this case, the composition of separated glass may not exactly represent the melt composition that was in equilibrium with the earlier crystallized plagioclase.

To avoid this influence of trace-element concentration of sanidine, partition coefficients were also calculated from the trace-element compositions of the whole rock and plagioclase in two different ways: equilibrium crystallization and Rayleigh fractional crystallization.

Equilibrium crystallization calculations assume that the plagioclase crystallized from the magma under equilibrium con-

Table 2a. Plagioclase/glass partition coefficients

Area		Italy	Thomas Range		Long Valley Caldera				California
Units		Lipari	Topaz Mountain		Glass Creek	Obsidian Dome	Deer Mt.	Punch Bowl	Clear Lake
Plagioclase wt%		0.50	2.5	4.5	22	3	17	2	1
Sample no.		98502*	98701*	98702*	98711*	98712	98713*	98717*	98721
$D^{\mathrm{pl/gl}}$		ICP	ICP	ICP	XRF	XRF	XRF	XRF	ICP
Partition coefficients (D) calculated from plagioclase and glass pairs: $D = C^{\mathrm{plag}} / C^{\mathrm{glass}}$									
Rb	$D^{\mathrm{pl/gl}}$				0.01 (<.01)	0.09 (0.01)	0.03 (<.01)	0.06 (0.01)	0.05 (<.01)
Sr		18.00 (1.06)	5.00 (0.28)	2.47 (0.14)	5.51 (0.31)	13.27 (0.76)	5.79 (0.33)	20.00 (1.15)	7.12 (0.41)
Ba		4.20 (0.21)	1.33 (0.06)	0.58 (0.02)	1.39 (0.06)	2.90 (0.14)	1.25 (0.06)	2.27 (0.11)	0.61 (0.03)
Y		0.07 (0.01)	0.10 (0.01)	0.11 (0.01)	0.21 (0.01)	0.16 (0.01)	0.17 (0.01)	0.15 (0.01)	0.12 (0.01)
Zr		0.55 (0.03)	0.24 (0.01)	0.36 (0.02)	0.08 (<.01)	0.08 (<.01)	0.10 (0.01)	0.08 (<.01)	0.04 (<.01)
Nb		0.12 (0.01)	0.09 (0.01)	0.09 (0.01)	n.d.	n.d.	n.d.	0.03 (<.01)	0.35 (0.04)
Th					n.d.	0.09 (0.01)	0.08 (0.01)	0.05 (<.01)	
La									
Ce									
Nd									
Partition coefficients (D) calculated from equilibrium crystallization fractionation: $D = C^{\mathrm{plag}} / [(C^{\mathrm{wr}} - nC^{\mathrm{plag}})/(1-n)]$									
Rb	D^{equ}				0.01 (<.01)	0.09 (0.01)	0.04 (<.01)	0.06 (0.01)	0.05 (<.01)
Sr		15.82 (0.91)	2.94 (0.16)	1.83 (0.10)	4.16 (0.24)	13.77 (0.79)	4.37 (0.25)	8.65 (0.50)	7.18 (0.41)
Ba		4.27 (0.20)	0.68 (0.03)	0.44 (0.02)	0.42 (0.02)	2.81 (0.13)	0.41 (0.01)	1.64 (0.08)	0.61 (0.03)
Y		0.07 (<.01)	0.09 (0.01)	0.10 (0.01)	0.19 (0.01)	0.14 (0.01)	0.16 (0.01)	0.13 (0.01)	0.11 (0.01)
Zr		0.50 (0.03)	0.23 (0.01)	0.38 (0.02)	0.04 (<.01)	0.08 (<.01)	0.05 (<.01)	0.08 (<.01)	0.05 (<.01)
Nb		0.12 (0.01)	0.09 (0.01)	0.07 (0.01)	n.d.	n.d.	n.d.	0.02 (<.01)	0.28 (0.03)
Th					n.d.	0.08 (<.01)	0.07 (<.01)	0.05 (<.01)	
La									
Ce									
Nd									
Partition coefficients (D) calculated from Rayleigh fractionation crystallization: $D = \mathrm{Ln}[(C^{\mathrm{wr}} - n^*C^{\mathrm{plag}})/C^{\mathrm{wr}}] / \mathrm{Ln}(1-n)$ (Korringa and Noble 1971)									
Rb	D^{ray}				0.02 (<.01)	0.09 (0.01)	0.04 (<.01)	0.06 (0.01)	0.05 (<.01)
Sr		15.26 (0.88)	2.87 (0.16)	1.79 (0.10)	3.13 (0.18)	11.65 (0.67)	3.43 (0.19)	8.37 (0.48)	6.97 (0.40)
Ba		4.23 (0.20)	0.68 (0.03)	0.45 (0.02)	0.45 (0.02)	2.73 (0.13)	0.44 (0.02)	1.63 (0.08)	0.61 (0.03)
Y		0.07 (<.01)	0.09 (0.01)	0.10 (0.01)	0.21 (0.01)	0.15 (0.01)	0.17 (0.01)	0.13 (0.01)	0.11 (0.01)
Zr		0.50 (0.03)	0.23 (0.01)	0.39 (0.02)	0.05 (<.01)	0.08 (<.01)	0.06 (<.01)	0.08 (<.01)	0.05 (<.01)
Nb		0.12 (0.01)	0.09 (0.01)	0.07 (0.01)	n.d.	n.d.	n.d.	0.02 (<.01)	0.28 (0.03)
Th					n.d.	0.09 (<.01)	0.08 (<.01)	0.05 (<.01)	
La									
Ce									
Nd									

Note: Numbers in parentheses represent standard errors, calculated by applying the method of Ragland (1989).
Italic numbers are calculated from ICP value. Bolded numbers are the corrected D from glass contamination for ECS.
* The samples with two feldspars. n.d. Not detectable.
Symbols used in this table: n = weight fraction of plagioclase in rock, C^{plag} = trace-element composition in plagioclase, C^{glass} = trace-element composition in glass/matrix, C^{wr} = Trace-element composition in whole rock.

TABLE 2B. Plagioclase/glass partition coefficients (continued)

Area		Brothers fault zone				South Sisters		Crater Lake		
Units		Frederic Butte		Elk Butte		Rock Mesa	Devils Hill	PHO LR	PHO CW	
Plagioclase wt%		20		2		8	7	6	8	
Sample no.		98801	98801	98802	98802	98807	98808	98811	98812	98812
$D^{pl/gl}$		XRF	ICP	XRF	ICP	XRF	ICP	ICP	XRF	ICP
Partition coefficients (*D*) calculated from plagioclase and glass pairs: $D = C^{plag} / C^{glass}$										
Rb	$D^{pl/gl}$	0.03 (<.01)	0.03	0.03 (<.01)	0.06	0.11 (0.01)		0.02 (<.01)	0.07 (0.01)	0.05
Sr		6.34 (0.37)	6.89	7.25 (0.42)	7.95	5.98 (0.34)	5.94 (0.34)	5.20 (0.30)	4.13 (0.24)	4.35
Ba		0.56 (0.03)	0.55	0.35 (0.02)	0.39	0.70 (0.03)	0.45 (0.02)	0.46 (0.02)	0.46 (0.02)	0.42
Y		0.07 (0.01)	0.03	0.03 (<.01)	0.06	0.08 (0.01)	0.07 (<.01)	0.02 (<.01)	0.00	0.04
Zr		0.00 (<.01)		0.01 (<.01)		0.15 (0.01)	0.09 (0.01)	0.00 (0.02)	0.00	
Nb		0.00	0.88	0.00	2.25	0.00	0.91 (0.10)	1.50 (0.16)	n.d.	1.40
Th		0.60 (0.04)		0.00		0.10 (<.01)			0.00	
La		0.31		0.33		0.36			0.20	
Ce		0.10		n.d.		0.09			0.13	
Nd		0.43		0.20		0.36			0.37	
Partition coefficients (*D*) calculated from equilibrium crystallization fractionation: $D = C^{plag} / [(C^{wr} - nC^{plag})/(1-n)]$										
Rb	D^{equ}	0.02 (<.01)		0.03 (<.01)		0.11 (0.01)		0.02 (<.01)	0.06 (0.01)	
Sr		8.68 (0.50)		6.09 (0.35)		5.28 (0.30)	5.90 (0.34)	4.63 (0.27)	3.95 (0.23)	
Ba		0.55 (0.03)		0.35 (0.02)		0.71 (0.03)	0.43 (0.02)	0.47 (0.02)	0.46 (0.02)	
Y		0.02 (<.01)		0.03 (<.01)		0.08 (0.01)	0.07 (<.01)	0.02 (<.01)	0.00	
Zr		0.00		0.01 (<.01)		0.15 (0.01)	0.09 (0.01)		0.00	
Nb		0.00		0.00		0.00	1.48 (0.15)	2.14 (0.22)	n.d.	
Th		0.71 (0.03)		0.00		0.10 (<.01)			0.00	
La		0.16		0.30		0.38			0.16	
Ce		0.03		n.d.		0.08			0.13	
Nd		0.12		1.00		0.32			0.39	
Partition coefficients (*D*) calculated from Rayleigh fractionation crystallization: $D = \mathrm{Ln}[(C^{wr} - n{*}C^{plag})/C^{wr}] / \mathrm{Ln}(1-n)$ (Korringa and Noble 1971)										
Rb	D^{ray}	0.03 (<.01)		0.03 (<.01)		0.11 (0.01)		0.02 (<.01)	0.07 (0.01)	
Sr		5.17 (0.30)		5.80 (0.33)		4.53 (0.26)	5.07 (0.29)	4.18 (0.24)	3.54 (0.20)	
Ba		0.58 (0.03)		0.35 (0.02)		0.72 (0.03)	0.44 (0.02)	0.48 (0.02)	0.47 (0.02)	
Y		0.03 (<.01)		0.03 (<.01)		0.08 (0.01)	0.07 (<.01)	0.02 (<.01)	0.00	
Zr		0.00		0.01 (<.01)		0.16 (0.01)	0.09 (0.01)		0.00	
Nb		0.00		0.00		0.001.45 (0.15)		2.07 (0.22)	n.d.	
Th		0.73 (0.04)		0.00		0.11 (0.01)			0.00	
La		0.18		0.30		0.39			0.17	
Ce		0.04		n.d.		0.08			0.13	
Nd		0.13		0.17		0.32			0.40	

ditions and that the weight fraction of plagioclase is equal to its volume percent. The coexisting magma composition was calculated from the formula:

$$C^{L} = (C^{0} - nC^{pl})/(1 - n) \quad (2)$$

where C^{L} is the glass/matrix composition, C^{0} is the initial magma composition assumed to be that of the whole-rock, C^{pl} is the plagioclase composition, and n is the weight fraction of plagioclase phenocrysts. The equilibrium partition coefficients were calculated using Equation 1. The results are listed in Table 2.

Because of zonation in plagioclase, only the surfaces of zoned phenocrysts were in equilibrium with the surrounding melt. Partition coefficients calculated from Equation 1—the direct comparison of crystal and coexisting glass/matrix composition—is the "apparent partition coefficient" (Albarede and Bottinga 1972), and is the average value representing a range from core to rim of the crystal. Therefore, the Rayleigh fractionation law should be considered in the calculation of partition coefficients (Greenland 1970; Korringa and Noble 1971). Equation 4 of Korringa and Noble (1971) was used in this calculation

$$D = \ln[(C^{0} - nC^{pl})/ C^{0}]/\ln(1 - n) \quad (3)$$

where D is the partition coefficient, and all others the same as Equation 2. In this calculation, only plagioclase and whole-rock compositions were used to avoid the influence of coexisting sanidine. Results are listed in Table 2.

When these three methods of calculation are compared, partition coefficients for compatible elements show some variation, whereas those for incompatible elements do not seem to be influenced by the method of calculation. For the compatible element Sr, partition coefficients calculated from Rayleigh Equation 3 (D^{ray}) are lower than those derived by plagioclase over glass/matrix ratio Equation 1 ($D^{pl/gl}$) (Fig. 1A). For Ba, which is incompatible or weakly compatible in plagioclase, D^{ray} is similar to $D^{pl/gl}$ (Fig. 1B). All the points that fall far off the reference line are from two-feldspar rocks. Partition coefficients calculated using equilibrium crystallization (Eq. 2, D^{equ}) and Rayleigh fractionation (Eq. 3, D^{ray}) are similar (Fig. 2). In the Sr plot (Fig. 2A), the points that lie off the reference line are those from highly porphyritic rocks (>10 vol% plagioclase). At low degrees of crystallization, the apparent partition coefficients are close to equilibrium partition coefficients (Albarede and Bottinga 1972). The difference between D^{ray} and D^{equ} for Ba is not very significant (Fig. 2B). This result implies that

TABLE 2C. Plagioclase/glasspartition coefficients (continued)

Area		Crater Lake				Taylor	Valles Caldera		
Units		PPO RD		PPO GH		Tt11/ SMC	SMR	SMR	SMR
Plagioclase wt%		13		12		1	6	3	5
Sample no.		98813	98813	98814	98814	98911*	93908B*	95811B*	98901*
$D^{pl/gl}$		XRF	ICP	XRF	ICP	ICP	ICP	ICP	ICP
Partition coefficients (D) calculated from plagioclase and glass pairs: $D = C^{plag} / C^{glass}$									
Rb	$D^{pl/gl}$	0.04 (<.01)	0.04	0.03 (<.01)	0.04				
Sr		6.71 (0.39)	7.44	7.11 (0.41)	6.95	10.67 (0.62)		9.63 (0.56)	22.63 (1.31)
Ba		0.53 (0.03)	0.54	0.50 (0.02)	0.47	11.81 (0.57)		2.62 (0.13)	5.47 (0.26)
Y		0.09 (0.01)	0.05	0.02 (<.01)	0.04	0.17 (0.01)		0.02 (<.01)	0.01 (<.01)
Zr		0.01 (<.01)		0.00		0.19 (0.01)		0.05 (<.01)	0.05 (<.01)
Nb		0.00	1.20	0.00	1.50	0.04 (<.01)		0.05 (<.01)	0.04 (<.01)
Th		0.29 (0.02)		0.22 (0.02)					
La		0.22		0.25					
Ce		n.d.		0.07					
Nd		0.14		0.20					
Partition coefficients (D) calculated from equilibrium crystallization fractionation: $D = C^{plag} / [(C^{wr}-nC^{plag})/(1-n)]$									
Rb	D^{equ}	0.04 (<.01)		0.03 (<.01)					
Sr		4.64 (0.27)		6.32 (0.36)		5.58 (0.32)	15.62 (0.90)	8.19 (0.47)	9.07 (0.52)
Ba		0.57 (0.03)		0.53 (0.03)		8.86 (0.43)	1.86 (0.09)	1.96 (0.09)	1.61 (0.08)
Y		0.08 (0.01)		0.01 (<.01)		0.13 (0.01)	0.02 (<.01)	0.01 (<.01)	0.01 (<.01)
Zr		0.01 (<.01)		0.00		0.21 (0.01)	0.04 (<.01)	0.04 (<.01)	0.05 (<.01)
Nb		0.00		0.00		0.03 (<.01)	0.04 (<.01)	0.04 (<.01)	0.04 (<.01)
Th		0.28 (0.05)		0.26 (0.01)					
La		0.22		0.25					
Ce		n.d.		0.06					
Nd		0.16		0.20					
Partition coefficients (D) calculated from Rayleigh fractionation crystallization: $D = \mathrm{Ln}[(C^{wr}-n^*C^{plag})/C^{wr}] / \mathrm{Ln}(1-n)$ (Korringa and Noble 1971)									
Rb	D^{ray}	0.05 (<.01)		0.03 (<.01)					
Sr		3.78 (0.22)		4.86 (0.28)		5.45 (0.31)	11.18 (0.65)	7.44 (0.48)	7.61 (0.49)
Ba		0.58 (0.03)		0.55 (0.03)		8.53 (0.41)	1.81 (0.09)	1.93 (0.09)	1.59 (0.08)
Y		0.09 (0.01)		0.01 (<.01)		0.13 (0.01)	0.02 (<.01)	0.01 (<.01)	0.01 (<.01)
Zr		0.01 (<.01)		0.00		0.21 (0.01)	0.05 (<.01)	0.04 (<.01)	0.05 (<.01)
Nb		0.00		0.00		0.03 (<.01)	0.04 (<.01)	0.04 (<.01)	0.04 (<.01)
Th		0.28 (0.06)		0.27 (0.02)					
La		0.24		0.26					
Ce		n.d.		0.07					
Nd		0.16		0.21					

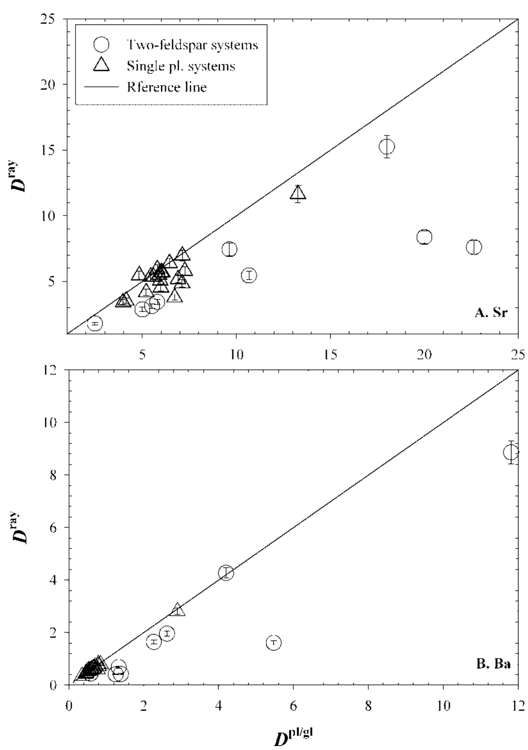

◀ **FIGURE 1.** Comparison of Sr (**a**) and Ba (**b**) partition coefficients calculated from the Rayleigh equation (D^{ray}) and those derived from plagioclase over glass/matrix ratio ($D^{pl/gl}$). For plagioclases from two-feldspar rocks (Lipari, Topaz Mountain, Long Valley, Taylor Creek, and South Mountain rhyolite), D^{ray} is lower than $D^{pl/gl}$ because Sr and Ba are compatible in sanidine. Error bars represent 1s percent deviation based on the coefficient of variation calculated from duplicate analyses of internal standards for XRF at Baylor University.

crystallization of plagioclase should be, at least, a process analogous to Rayleigh fractionation.

For incompatible elements (Rb, Y, Zr, and Th), D^{ray} values are close to $D^{pl/gl}$ (Fig. 3). The weak deviation from the reference line could be caused by analytical error. Values of D^{ray} are almost equal to D^{equ} (Table 2).

Through the above comparisons, we can see that fractionation of sanidine has a dramatic influence on the partition coefficients of compatible trace elements in plagioclase. Directly calculated ratios for these compatible elements could not represent the equilibrium partition coefficients of plagioclase if the system has suffered sanidine fractionation. Incompatible trace elements are weakly influenced by coexisting sanidine. The influence on partition coefficients from the zonation of plagioclase can only be observed in compatible elements where the rocks are highly porphyritic.

TABLE 2D. Plagioclase/glass partition coefficients (continued)

Area		Valles Caldera											
Units		El Cajete					Battleship Rock Tuff			Banco Bonito			
Plagioclase wt%		5	3		5	5	5	4	4	5		5	
Sample no.		93907	95821	95821	95824	95825	95525	95801	95802	93904B	93904B	95524	95524
$D^{pl/gl}$		XRF	XRF	ICP	XRF	XRF	ICP	XRF	ICP	XRF	ICP	XRF	ICP
Partition coefficients (*D*) calculated from plagioclase and glass pairs: $D = C^{plag} / C^{glass}$													
Rb	$D^{pl/gl}$	0.23	0.24		0.25	0.21		0.25		0.20		0.21	
Sr		5.07	4.77	4.14	4.44	4.89	5.25	5.63	3.83	5.30	3.82	5.16	4.59
Ba		0.66	0.70	0.67	0.62	0.71	0.82	0.73	0.86	0.80	0.81	0.82	0.79
Y		0.22	0.31	0.12	0.30	0.21	0.15	0.28	0.03	0.24	0.05	0.27	0.09
Zr		0.19	0.29	0.30	0.30	0.19	0.29	0.30	0.12	0.21	0.06	0.19	0.30
Nb		0.00	n.d.	0.19	n.d.	0.00	0.26	n.d.	0.10	n.d.	0.12	n.d.	0.18
Th		0.25	0.23		0.14	0.25			0.18		0.22		0.20
La		0.50				0.53							
Ce		0.33				0.29							
Nd		0.41				0.35							
Partition coefficients (*D*) calculated from equilibrium crystallization fractionation: $D = C^{plag} / [(C^{wr}–nC^{plag})/(1–n)]$													
Rb	D^{equ}	0.23	0.25		0.25	0.21		0.25		0.20		0.21	
Sr		5.67	5.38		5.22	5.07	5.25	6.15	3.40	5.47		5.38	
Ba		0.64	0.68		0.62	0.71	0.76	0.70	0.80	0.61		0.82	
Y		0.24	0.24		0.24	0.22	0.13	0.25	0.03	0.20		0.24	
Zr		0.15	0.21		0.21	0.14	0.21	0.22	0.10	0.17		0.15	
Nb		0.00	*0.19*		n.d.	0.00	0.30	n.d.	0.13	*0.13*		*0.17*	
Th		0.23	0.28		0.14	0.25		0.18		0.29		0.21	
La		0.45			0.51								
Ce		0.28			0.28								
Nd		0.40			0.32								
Partition coefficients (*D*) calculated from Rayleigh fractionation crystallization: $D = \text{Ln}[(C^{wr}–n^{*}C^{plag})/C^{wr}] / \text{Ln}(1–n)$ (Korringa and Noble 1971)													
Rb	D^{ray}	0.23	0.25		0.25	0.22		0.26		0.20		0.21	
Sr		5.09	4.86		4.73	4.61	4.94	5.47	3.28	4.84		4.68	
Ba		0.65	0.68		0.63	0.71	0.77	0.70	0.80	0.62		0.83	
Y		0.25	0.24		0.25	0.22	0.13	0.26	0.03	0.20		0.25	
Zr		0.15	0.21		0.21	0.15	0.21	0.23	0.10	0.17		0.16	
Nb		0.00	*0.19*		n.d.	0.00	0.30	n.d.	0.13	*0.13*		*0.18*	
Th		0.23	0.28		0.14	0.26		0.19		0.29		0.22	
La		0.46			0.52								
Ce		0.28			0.28								
Nd		0.40											

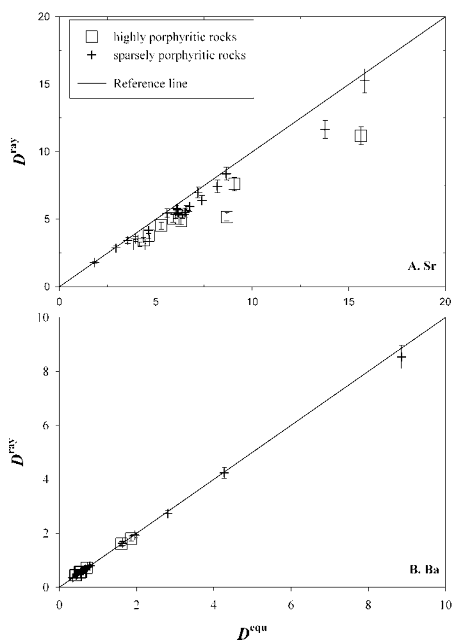

FIGURE 2. Comparison of Sr (**a**) and Ba (**b**) partition coefficients calculated from the Rayleigh equation (D^{ray}) and those calculated from the equilibrium equation (D^{equ}). For Sr, D^{ray} are lower than D^{equ} only in the highly porphyritic rocks (one sample from Brother Fault Zone, two samples from Long Valley caldera, and two samples from Crater Lake). For Ba, D^{ray} is nearly equal to D^{equ}.

We conclude that partition coefficients calculated from Rayleigh fractional crystallization are the most suitable numbers to be used in this plagioclase partitioning study. All the partition coefficients discussed in the following part of this paper are partition coefficients calculated assuming Rayleigh fractionation (Eq. 3) (Table 2).

Influence factors on plagioclase partition coefficients

Previous studies indicate that D_{Sr} and D_{Ba} have negative relationships with the An content in plagioclase, implying that crystal chemistry is the major control on the Sr and Ba partitioning between plagioclase and silicic melt (Blundy and Wood 1991). Values of D_{Sr} and D_{Eu} are strongly dependent upon temperature (Drake 1972; Sun et al. 1974; Drake and Weill 1975). However, bulk composition of the system may also affect distribution coefficients (Sun et al. 1974; Masuda and Kushiro 1970). This study will discuss the influence of plagioclase and host rock major-element compositions and, where available, temperature on partition coefficients.

Strontium

The variation of D_{Sr} with anorthite content (An) of host plagioclase is shown in Figure 4A. There are two different trends between D_{Sr} and An, both of them showing a positive correlation, but with different slopes. With increasing An, one group (T1) mainly has $D_{Sr} > 6$ and shows steep-sloped trend, and another group (T2) mainly has $D_{Sr} < 6$ and a gently sloped trend.

TABLE 2E. Plagioclase/glass partition coefficients (continued)

Area		Valles Caldera								
Units		El Cajete				Battleship Rock Tuff			Banco Bonito	
Sample no.		93907	95821	95824	95825	95525	95801	95802	93904B	95524
$D^{pl/gl}$		XRF	XRF	XRF	XRF	ICP	XRF	ICP	XRF	XRF
Correction of glass contamination for ECS										
Partition coefficients (*D*) calculated from plagioclase and glass pairs: *D* = C^{plag} / C^{glass}										
Rb	$D^{pl/gl}$	**0.10** (0.01)	**0.11** (0.01)	**0.12** (0.01)	**0.07** (0.01)		**0.12** (0.01)		**0.05** (0.00)	**0.07** (0.01)
Sr		**5.79** (0.33)	**5.44** (0.31)	**4.83** (0.28)	**5.58** (0.32)	**6.00** (0.35)	**6.44** (0.37)	**3.97** (0.23)	**6.06** (0.35)	**5.89** (0.34)
Ba		**0.60** (0.03)	**0.65** (0.03)	**0.55** (0.03)	**0.66** (0.03)	**0.79** (0.04)	**0.68** (0.03)	**0.85** (0.04)	**0.77** (0.04)	**0.79** (0.04)
Y		**0.08** (0.01)	**0.19** (0.01)	**0.18** (0.01)	**0.07** (<.01)	**0.01** (<.01)	**0.15** (0.01)	**0.03** (<.01)	**0.10** (0.01)	**0.15** (0.01)
Zr		**0.05** (<.01)	**0.17** (0.01)	**0.18** (0.01)	**0.05** (<.01)	**0.16** (0.01)	**0.18** (0.01)	**0.08** (<.01)	**0.07** (<.01)	**0.05** (<.01)
Nb			***0.05*** (<.01)			**0.13** (0.01)		**0.06** (0.01)	***0.03*** (<.01)	***0.04*** (<.01)
Th		**0.12** (0.01)	**0.10** (0.01)		**0.12** (0.01)		**0.04** (<.01)		**0.08** (<.01)	**0.06** (<.01)
La		**0.41**			**0.44**					
Ce		**0.21**			**0.17**					
Nd		**0.30**			**0.23**					
Partition coefficients (*D*) calculated from equilibrium crystallization fractionation: *D* = C^{plag} / [(C^{wr}–*n*C^{plag})/(1–*n*)]										
Rb	D^{equ}	**0.10** (0.01)	**0.11** (0.01)	**0.12** (0.01)	**0.07** (0.01)		**0.12** (0.01)		**0.05** (<.01)	**0.07** (0.01)
Sr		**6.76** (0.39)	**6.38** (0.37)	**6.15** (0.35)	**6.01** (0.35)	**6.14** (0.35)	**7.39** (0.43)	**3.55** (0.20)	**6.58** (0.38)	**6.52** (0.38)
Ba		**0.58** (0.03)	**0.63** (0.03)	**0.55** (0.03)	**0.65** (0.03)	**0.73** (0.04)	**0.65** (0.03)	**0.79** (0.04)	**0.58** (0.03)	**0.79** (0.04)
Y		**0.09** (0.01)	**0.14** (0.01)	**0.14** (0.01)	**0.07** (<.01)	**0.00** (0.00)	**0.14** (0.01)	**0.03** (<.01)	**0.08** (0.01)	**0.13** (0.01)
Zr		**0.04** (<.01)	**0.12** (0.01)	**0.12** (0.01)	**0.04** (<.01)	**0.12** (0.01)	**0.13** (0.01)	**0.06** (<.01)	**0.06** (<.01)	**0.04** (<.01)
Nb			***0.05*** (<.01)			**0.15** (0.02)		**0.07** (0.01)	***0.03*** (<.01)	***0.04*** (<.01)
Th		**0.11** (0.01)	**0.11** (0.01)		**0.12** (0.01)	**0.04** (<.01)			**0.11** (0.01)	**0.06** (<.01)
La		**0.37**			**0.43**					
Ce		**0.18**			**0.16**					
Nd		**0.29**			**0.21**					
Partition coefficients (*D*) calculated from Rayleigh fractionation crystallization: *D* = Ln[(C^{wr}–*nC^{plag})/C^{wr}] / Ln(1–*n*) (Korringa and Noble 1971)**										
Rb	D^{ray}	**0.10** (0.01)	**0.11** (0.01)	**0.12** (0.01)	**0.07** (0.01)		**0.12** (0.01)		**0.06** (<.01)	**0.07** (0.01)
Sr		**5.93** (0.34)	**5.37** (0.31)	**5.47** (0.32)	**5.36** (0.31)	**5.71** (0.33)	**6.40** (0.37)	**3.42** (0.20)	**5.67** (0.33)	**5.50** (0.32)
Ba		**0.59** (0.03)	**0.63** (0.03)	**0.56** (0.03)	**0.66** (0.03)	**0.74** (0.04)	**0.66** (0.03)	**0.79** (0.04)	**0.59** (0.03)	**0.80** (0.04)
Y		**0.09** (0.01)	**0.15** (0.01)	**0.15** (0.01)	**0.07** (<.01)	**0.00** (<.01)	**0.14** (0.01)	**0.03** (<.01)	**0.09** (0.01)	**0.13** (0.01)
Zr		**0.04** (<.01)	**0.12** (0.01)	**0.12** (0.01)	**0.04** (<.01)	**0.12** (0.01)	**0.13** (0.01)	**0.06** (<.01)	**0.06** (<.01)	**0.04** (<.01)
Nb			***0.05*** (0.01)		**0.15** (0.02)			**0.07** (0.01)	***0.03*** (<.01)	***0.05*** (<.01)
Th		**0.11** (0.01)	**0.12** (0.01)		**0.12** (0.01)		**0.04** (<.01)	**0.11** (0.01)	**0.06** (<.01	
La		**0.38**			**0.43**					
Ce		**0.18**			**0.16**					
Nd		**0.30**			**0.22**					

Note: Bolded numbers are the corrected D from glass contamination for ECS.

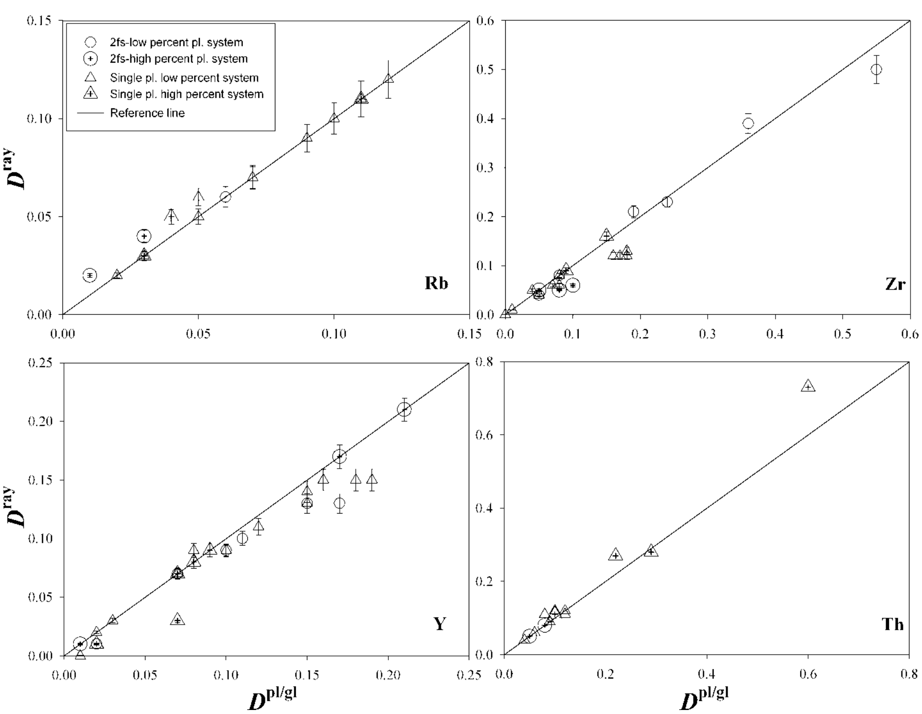

FIGURE 3. Comparison of Rb, Y, Zr, and Th partition coefficients calculated from the Rayleigh equation (D^{ray}) and those derived from the plagioclase over glass/matrix ratio ($D^{pl/gl}$). D^{ray} are similar to $D^{pl/gl}$. The partitioning of incompatible trace elements is not obviously influenced by coexisting minerals or the zonation of plagioclase. Symbols: open circle = two-feldspar system with low volume percent plagioclase; circle with cross = two-feldspar system with high volume percent plagioclase; open triangle = single plagioclase system with low volume percent plagioclase; triangle with cross = single plagioclase system with high volume percent plagioclase.

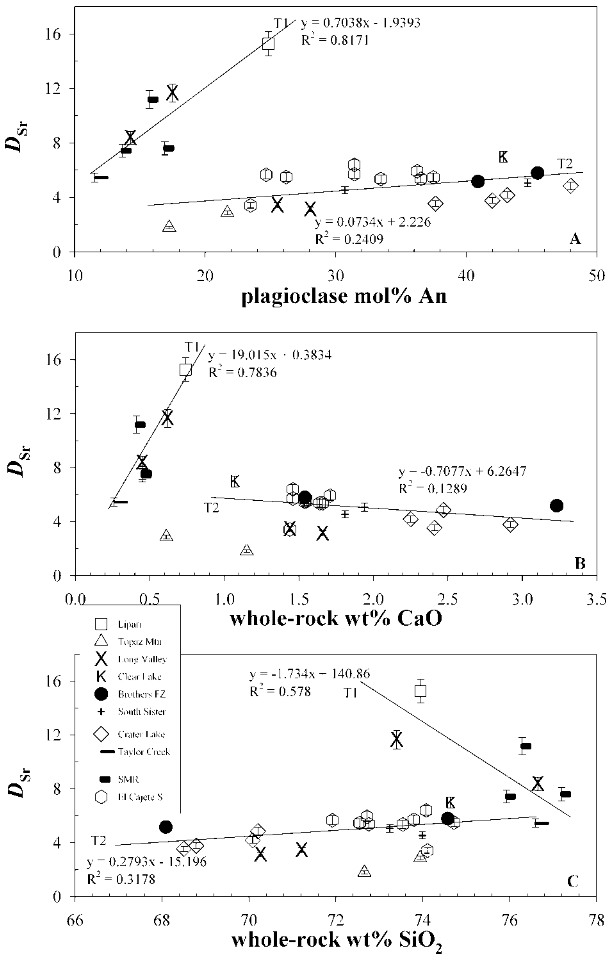

FIGURE 4. Two different trends (T1 and T2) in partition coefficients of Sr. (**a**) D_{Sr} vs. plagioclase mol% An. Both trends show positive relationships between D_{Sr} and An. (**b**) D_{Sr} vs. whole-rock wt% CaO. High D_{Sr} samples (T1) fall in low-CaO range (CaO < 1 wt%); low D_{Sr} samples (T2) fall in high-CaO range. Samples from Thomas Range (triangles in squares) were not included in the linear regression. (**c**) D_{Sr} vs. whole-rock wt% SiO_2. High D_{Sr} samples (T1) fall in high-silica range. Samples from Thomas Range (triangles in squares) were not included in the linear regression. Symbols: solid square = Lipari, Italy; triangle = Topaz Mountain rhyolite, Thomas Range, Utah; X = Long Valley Caldera, California; K = Clear Lake, California; solid circle = rhyolite domes from Brothers Fault Zone, Oregon; cross = South Sister, Oregon; diamond = Crater Lake, Oregon; long bar = Taylor Creek Rhyolite, New Mexico; short bar = South Mountain rhyolite, Valles Caldera, New Mexico; and hexagon = El Cajete Series, Valles Caldera, New Mexico.

Group T1 is also characterized by low whole-rock CaO (<1 wt%) and high SiO_2, whereas group T2 contains higher CaO and lower SiO_2 (Figs. 4B, 4C). Also, high D_{Sr} occurs mainly in low-Sr and plagioclase-poor rocks. Through principal-component and multiple linear regression analysis, it was determined that the major influences on Sr partitioning are from plagioclase (CaO content) and whole-rock composition (SiO_2, CaO, and K_2O). As expected, the Sr content in the magma has influence on the Sr content in plagioclase. Temperature shows a strong correlation with D_{Sr} in the T2 group.

Mysen (1976, 1978) demonstrated that trace-element partition coefficients increase, in general, with decreasing concentration at low trace-element contents and do not obey Henry's law. Drake and Holloway (1978) mentioned that experimental procedures could have a critical influence on low trace-element content partitioning. Bindeman and Davis (2000) showed that D_{REE} increased 50–100% with decreasing total REE. Our data show that high D_{Sr} characterizes in low-Sr rocks, but the highest D_{Sr} is not from the rock with the lowest Sr. Therefore, the high D is not due to the failure of Henry's law. It has been suggested that the plagioclase crystal structure prefers Sr to Ca (Higuchi and Nagasawa 1969). If this is the case, the highest D_{Sr} should be accompanied by the lowest Sr content in whole-rock system. According to our data, D_{Sr} increases with decreasing SrO/CaO ratio of the whole rock, except Topaz Mountain rhyolite. In fact, SrO/CaO in plagioclase is similar to that of the whole rock. The atomic radii are also similar for Sr^{2+} and Ca^{2+} (eightfold-coordinated ionic radii are 1.26 and 1.12 Å, respectively; Shannon 1976). This pattern means that Sr and Ca should have the same opportunity to enter the plagioclase structure.

The CaO content of the whole rock may have a major influence on Sr partitioning. Where the high-Al felsic magma systems have low CaO, the concentration of other 2 + cations (such as Sr) in plagioclase could cause the high partitioning of those elements. Because these systems also have low Sr content, they are more sensitive to compositional variation; the concentration of Sr in plagioclase will result in high Sr partition coefficients.

Samples from the Topaz rhyolite are generally off the trends (Figs. 4B, 4C), which perhaps is related to the high volatile content of the rock (Christiansen et al. 1984). High F and Cl in the Topaz rhyolite may favor the formation of high-charge cation complexes in the liquid, which might inhibit Sr from entering plagioclase.

Barium

Barium is generally incompatible in plagioclase, whereas in some high-silica rhyolites, Ba becomes compatible. In this study, D_{Ba} ranges from 0.35 to 8.53. A plot of D_{Ba} vs. the An content of plagioclase (Fig. 5A) show two trends: one positive with $D_{Ba} > 1$ (mainly in plagioclase < 20 mol% An, T1); another slightly negative with $D_{Ba} < 1$ (T2). One Taylor Creek rhyolite with high D_{Ba} is anomalous and possibly erroneous, and is not plotted in the figures. High D_{Ba} samples have low total Ba, and generally are less plagioclase phyric.

Magma compositions could strongly influence D_{Ba}. High D_{Ba} samples are found mainly in rocks with high silica contents (73.4–77.2 wt% SiO_2, Fig. 5B). All high D_{Ba} samples are from low-Ca rocks (<1 wt% CaO), and correlate positively with CaO (Fig. 5C). In higher CaO rocks, the variation of CaO slightly influences the partitioning of Ba. The high D_{Ba} samples also have high whole-rock K_2O (Fig. 5D). Topaz Mountain rhyolite, despite having high K_2O, has low D_{Ba}.

BaO/K_2O and BaO/CaO in plagioclase are both low for high D_{Ba} samples, and correspond with low BaO/K_2O and BaO/CaO

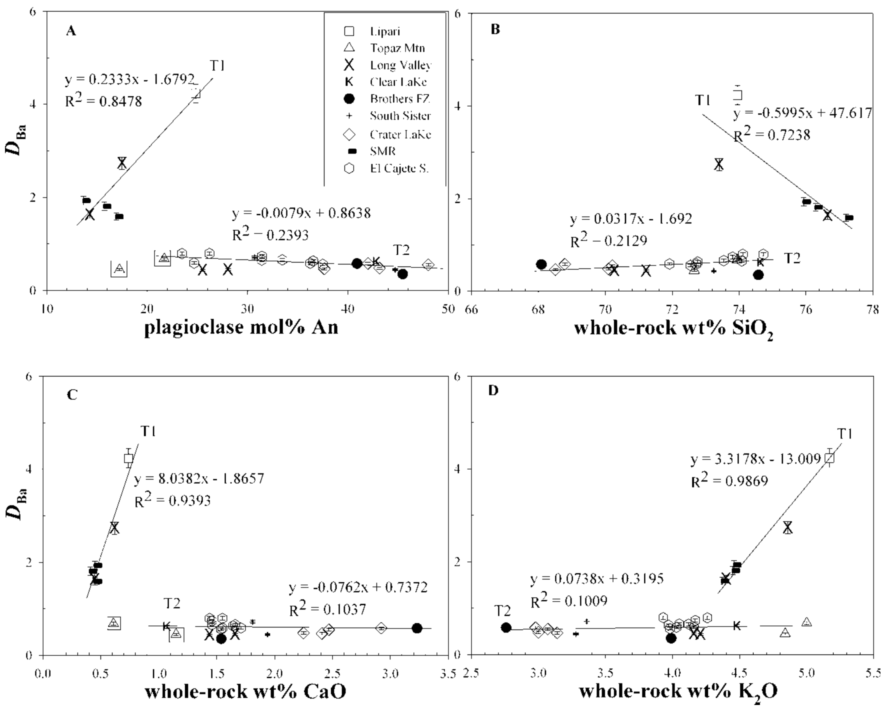

FIGURE 5. D_{Ba} relationships with plagioclase composition and whole-rock Ba content. (**a**) High D_{Ba} samples correlate positively with mol% An (T1); low D_{Ba} trend has a weak negative relationship with mol% An (T2). Samples from Thomas Range (triangles in squares) were not included in the linear regression. (**b**) High D_{Ba} samples concentrate in high silica rocks. (**c**) High D_{Ba} samples have low whole-rock CaO (<1 wt%) and correlate positively with wt% CaO (T1). Low D_{Ba} samples (T2) show a flat pattern. (**d**) High D_{Ba} samples have high whole-rock wt% K_2O. Symbols same as Figure 4.

ratios in the whole rock. Therefore, in low Ba systems, high D_{Ba} results from an elevated Ba content in plagioclase. BaO/K_2O ratios in plagioclase are larger than those of the whole rock. This finding implies that the plagioclase structure favors the smaller radius and higher charge Ba^{2+} cation over K^+ (eight-fold-coordinated ionic radii are 1.42 and 1.51 Å, respectively; Shannon 1976) in our systems. BaO/CaO ratios are smaller in plagioclase than in whole rock. The abundance of Al in these Al-oversaturated magmas would facilitate Ba^{2+} substitution.

The feldspar structure could be another influence on Ba partitioning. The relative elasticity of the crystal site is the major control for the entry of large cations (Brice 1975). The high-albite plagioclase structure is more flexible because of their larger M-site (Angel et al. 1988). Through the study of anorthite-rich and anorthite-poor plagioclase (Bindeman et al. 1998), partition coefficients of larger cations show a significant increase in higher albite plagioclase (Bindeman and Davis 2000; Blundy and Wood 1991). Therefore, Ba can become compatible in the low CaO, high Al_2O_3 systems.

According to principal-component and multiple regression analysis, the major influences for Ba partitioning are from both plagioclase (wt% CaO and K_2O) and whole-rock composition (SiO_2, Al_2O_3, CaO, and K_2O). In addition, the Ba content in the magma also strongly influences the Ba content in plagioclase. Temperature shows a strong correlation with D_{Ba} in both groups.

Of all these factors, the CaO content of peraluminous magmas could be the major influence on the appearance of two trends. In highly evolved, high-silica, peraluminous systems, a low CaO content in the magma results in low An in plagioclase, but high Al in the system may cause more Al for Si substitution in the plagioclase and the need for higher charge cations. This effect could allow Ba to enter plagioclase in lieu of Ca, and thus Ba could become compatible.

Correlation between D_{Sr} and D_{Ba}

There is a positive relationship between D_{Sr} and D_{Ba} (Fig. 6A). This correlation is better in the high partition coefficient range and less constrained for low values of D. The reason might be that, for high values of D, Ba and Sr both correlate with Ca in plagioclase, but for low D-values, D_{Ba} might correlate more with K in plagioclase. Two samples of Topaz Mountain rhyolite have both low D_{Sr} and low D_{Ba}. This feature may be the result of high volatile content in the magma, as discussed above in the Sr section.

In plots of D_{Sr} and D_{Ba} vs. temperature (Figs. 6B, 6C), the low-D group (T2) correlates positively with temperature; however, the high-D group does not show such a trend. Temperature does not show an obvious influence on incompatible trace elements (Rb, Y, and Zr).

Other elements

Rubidium. Rubidium is incompatible in plagioclase, with D_{Rb} ranging from 0.02 to 0.25. D_{Rb} shows a weak positive correlation with the Or content of plagioclase (Fig. 7A) and with whole-rock SiO_2. D_{Rb} is higher in the lower-An plagioclase, but the variations are broad as described by Bindeman et al. (1998).

Yttrium. Yttrium variation mainly correlates with Ca because these cations have similar sizes (Lambert and Holland 1974). The ratio of Y_2O_3/CaO between plagioclase and magma shows a weak positive correlation in our systems (Fig. 7B).

D_Y seems to be different in different rock series. For example, metaluminous and peraluminous samples fall on separate trends (Fig. 7C), and D_Y decreases with increasing whole-rock silica contents in both groups.

Light REE and high field-strength elements (HFSE). Lanthanum, Ce, and Nd were analyzed by XRF in this study.

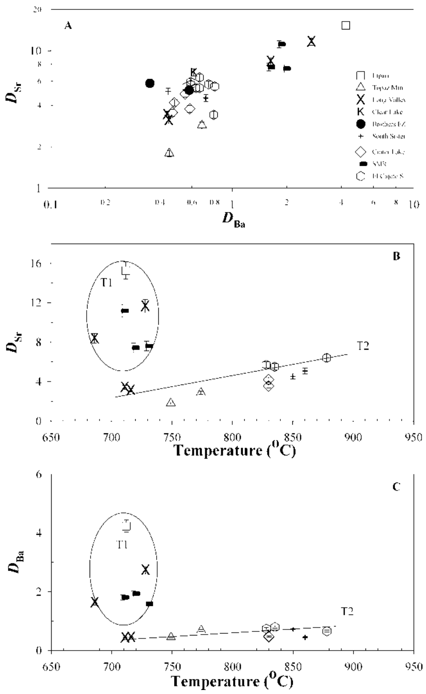

FIGURE 6. D_{Sr} and D_{Ba} relations and temperature influences on Sr and Ba partitioning. (**a**) D_{Sr} and D_{Ba} show a positive correlation, especially for high D_{Sr} and D_{Ba} group. (**b**) D_{Sr} shows a positive correlation with temperature for the T2 group, but not for the T1 group. (**c**)The relationship between D_{Ba} and temperature is similar to D_{Sr}. Symbols same as Figure 4.

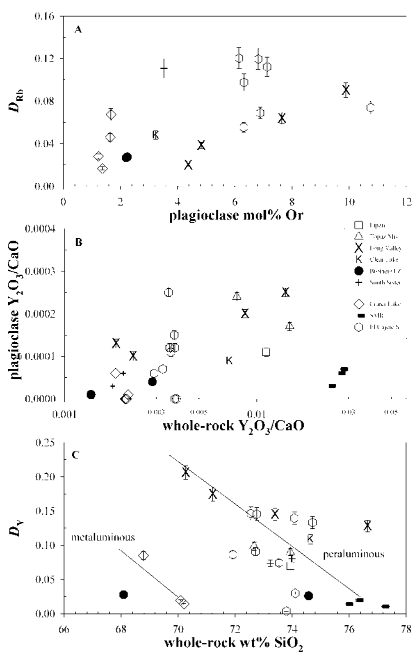

FIGURE 7. Correlation for Rb and Y. (**a**) D_{Rb} shows weakly positive relation with the mol% Or in plagioclase. (**b**) Y_2O_3/CaO between plagioclase and magma shows a weak-positive correlation. (**c**) D_Y decreases with increasing of whole-rock wt% SiO_2. Note that there are two trends: one for peraluminous rocks and another one for metaluminous rocks. Symbols same as Figure 4.

Lanthanum and Ce determined by XRF agree fairly well with ICP-MS analyses (Appendix II). Scatter in Nd reflects greater analytical error in the XRF data compared to ICP-MS data.

D_{La} and D_{Ce} correlate positively with whole-rock SiO_2 (Fig. 8A), negatively with whole-rock CaO (Fig. 8B), and positively with plagioclase Or (Fig. 8C). D_{LREE} increase with decreasing An in plagioclase, in agreement with published data (Drake and Weill 1975; Simon et al. 1994; Bindeman et al. 1998; Bindeman and Davis 2000). Partition coefficients for Ce are lower than for La and Nd, even though the contents of Ce in the whole-rock samples are higher than those of La and Nd (Appendix I). The oxidation state and radii of cations play an important role in the partitioning of Ce (Bindeman and Davis 2000). The smaller radius of Ce^{4+} compared with Ce^{3+} (Shannon 1976) may be the major reason for these lower values of D_{Ce}.

HFSE in our data set do not show clear relationships with either whole-rock or plagioclase compositions.

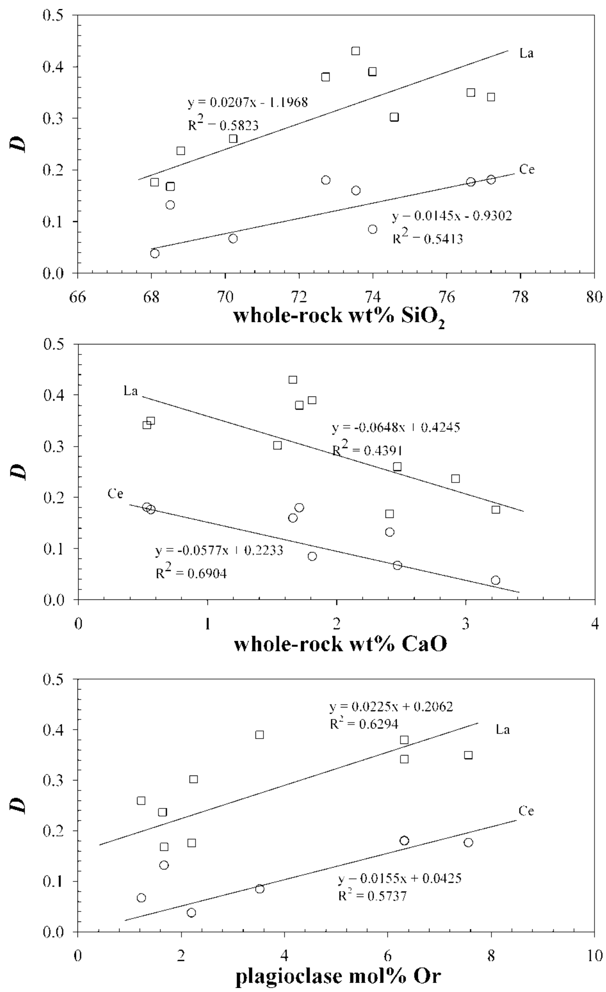

FIGURE 8. D_{La} and D_{Ce} vs. whole-rock composition. (**a**) D_{La} and D_{Ce} correlate positively with whole-rock wt% SiO_2. (**b**) D_{La} and D_{Ce} correlate negatively with whole-rock wt% CaO. (**c**) D_{La} and D_{Ce} correlate positively with mol% Or in plagioclase. Symbols: open square = D_{La}, open circle = D_{Ce}.

TABLE 3. Empirical equations for Sr, Ba, La, and Ce

Element	Whole-rock type	Least-squares regression equation	Formula no.	R-square	Standard error	F probability	Sample no.
Sr	CaO (wr) >1%	$D_{Sr} = 0.0806X_{An}–0.0102Sr^{(wr)} + 4.2327$ D_{Sr} with mol% An in plagioclase and whole-rock Sr concentration of all high-Ca samples, only Topaz Mountain rhyolite excluded. The results of this model are compared with published values. Agreement is good, except for high D_{Sr} values from Nash and Crecraft (1985).	(4a)	0.8537	0.3723	1.0000	20
		$D_{Sr} = 0.0393X_{An}–0.0071Sr^{(wr)} + 0.0064$ T(°C)–0.312 Adding temperature as a factor, better regression.	(4b)	0.9373	0.2440	0.9970	9
Ba	CaO (wr) >1%	$D_{Ba} = 1.2447–0.0093X_{An}–0.000393Ba^{(wr)}$ D_{Ba} with mol% An in plagioclase and the Ba (ppm) content in whole rock	(5a)	0.7939	0.0622	1.0000	18
		$D_{Ba} = 1.118–0.0136X_{An}$ D_{Ba} with mol% An in plagioclase, this equation is used in prediction because some published data did not have whole-rock Ba values. Results of this model are compared with published data. Agreement fairly good , except for some values from New Zealand (Ewart and Taylor, 1969), two samples from Japan (Nagasawa and Schnetzler 1971), and some D_{Ba} >1 values from Nash and Crecraft (1985).	(5b)	0.6130	0.0825	0.9997	18
		$D_{Ba} = 0.0571SiO_2^{(pl)} + 0.4198K_2O^{(pl)} + 0.0017T(°C) + 0.5992CaO^{(wr)} –5.5886$ $SiO_2^{(pl)}$ and $K_2O^{(pl)}$ are wt% SiO_2 and K_2O in plagioclase, $CaO^{(wr)}$ is wt% CaO in whole rock, T(°C) is the temperature in Celsius.	(5c)	0.9413	0.0503	0.9960	10
La		$D_{La} = 0.0137Or^{(pl)} + 0.0227SiO_2^{(wr)}–1.3732$ D_{La} with mol% Or in plagioclase and SiO_2 wt% in whole rock.	(6)	0.8936	0.0379	0.9953	8
Ce		$D_{Ce} = 0.0049Or^{(pl)}–0.0486CaO^{(wr)} + 0.1956$ DCe with mol% Or in plagioclase and CaO wt% in whole rock.	(7)	0.6381	0.0428	0.7822	6

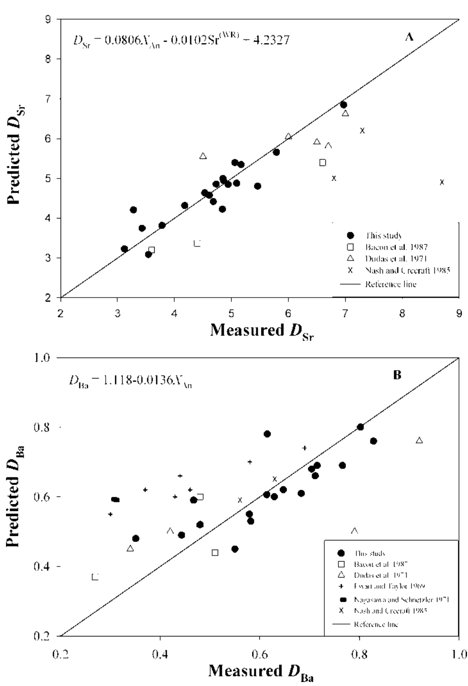

FIGURE 9. Results of Sr and Ba empirical prediction for high CaO systems. (**a**) Sr empirical correlation. Agreement is good, except for some high D_{Sr} values from Nash and Crecraft (1985). Key to literature data: open square, Bacon et al. (1987); open triangle, Dudas et al. (1971); and x, Nash and Crecraft (1985). (**b**) Ba empirical correlation. The equation used in this plot is $D_{Ba} = 1.118–0.0136X_{An}$ because of the absence of Ba values in some of published data. There is fairly good agreement, except that some predicted values from New Zealand (Ewart and Taylor 1969) and two samples from Japan (Nagasawa and Schnetzler 1971) are higher than published values. In addition, some values from Nash and Crecraft (1985) with D_{Ba}> 1 fail to be predicted by the model equation. Key to literature data: open square = Bacon et al. (1987); open triangle = Dudas et al. (1971); cross = Ewart and Taylor (1969); bar = Nagasawa and Schnetzler (1971); and x = Nash and Crecraft (1985).

EMPIRICAL CORRELATION

Because available plagioclase partition coefficients for Rb, Y, and high field-strength elements (HFSE) show no systematic correlation with melt or mineral composition, we cannot evaluate their variation. Only Sr, Ba, and LREE can be evaluated with the data of this study.

As discussed above, factors other than plagioclase influence partition coefficients. Therefore, it is inappropriate to use only plagioclase compositions to predict Sr and Ba partition coefficients. Multiple regression correlation between partition coefficients and mineral and/or magma compositions is used in our equations. The results for high-Ca systems (T2) are listed in Table 3.

The equations:

$D_{Sr} = 0.0806X_{An}–0.0102Sr^{(wr)} + 4.2327$

and

$D_{Ba} = 1.118 – 0.0136X_{An}$

are used to predict the published data (Figs. 9A, 9B). Agreements are fairly good and the results are listed in Appendix VI[1]. A simple D_{Ba} equation is used here because there were not enough published data for a multiple regression analysis.

Most published D-values for low-CaO systems, such as the Bishop Tuff, were calculated using INAA analyses, but published high-quality data are insufficient to build predictive equations for D_{Sr} and D_{Ba} in these low-CaO (T1) systems. The equations used in our study to generate the T1 calibration are listed on Figures 4 and 5. Additional study is needed for these systems.

ACKNOWLEDGMENTS

We thank T. Goforth, S. Dworkin, and K. Park for reviewing an early version of the manuscript. We are grateful to J. Icenhower, W. Leeman, J. Ayers, R. Dymek, and an anonymous reviewer for their constructive and helpful reviews and valuable comments. We also thank M. Barnes for the providing of ICP-AES analyses.

REFERENCES CITED

Albarede, F. (1975) Some trace element relationships among liquid and solid phases in the course of the fractional crystallization of magmas. Geochimica et Cosmochimica Acta, 40, 667–673.

Albarede, F. and Bottinga, Y. (1972) Kinetic disequilibrium in trace element partitioning between phenocrysts and host lava. Geochimica et Cosmochimica Acta, 36, 141–156.

Angel, R.J., Hazen, R.M., McCormick, T.C., Prewitt, C.T., and Smyth, J.R. (1988) Comparative compressibility of end-member feldspars. Physics and Chemistry of Minerals, 15, 313–318.

Arth, J.G. (1976) Behavior of trace elements during magmatic processes—a summary of theoretical models and their applications. U.S. Geological Survey Journal of Research, 4, 41–47.

Auwera, J.V., Longhi, J., and Duchesne, J.C. (2000) The effect of pressure on D_{Sr} (plag/melt) and D_{Cr} (Oxp/melt): implications for anorthosite petrogenesis. Earth and Planetary Science Letters, 178, 303–314.

Bacon, C.R. (1983) Eruptive history of Mount Mazama and Crater Lake caldera, Cascade Range, USA. Journal of Volcanology and Geothermal Research, 18, 57–115.

Bacon, C.R. and Druitt, T.H. (1988) Compositional evolution of the zoned calcalkaline magma chamber of Mount Mazama, Crater Lake, Oregon. Contributions to Mineralogy and Petrology, 98, 224–256.

Bacon, C.R., Hildreth, W., and Druitt, T.H. (1987) Partition coefficients determined from phenocryst and glass analyses of climactic eject of Mount Mazama, Oregon. 5 p. United States Geological Survey Open File Report, 87:589.

Bailey, R.A., Macdonald, R.A., and Thomas, J.E. (1983) The Inyo-Mono craters: Products of an actively differentiating rhyolite magma chamber, eastern California (abstract). EOS Transactions, American Geophysical Union, 64, 336.

Beattie, P., Drake, M.J., Jones, J., Leeman, W., Longhi, J., McKay, G., Nielsen, R., Palme, H., Shaw, D., Takahashi, E., and Watson, B. (1993) Terminology for trace-element partitioning. Geochimica et Cosmochimica Acta, 57, 1605–1606.

Berlin, R. and Henderson, C.M.B. (1969) The distribution of Sr and Ba between the alkali feldspar, plagioclase and groundmass phases of porphyritic trachytes and phonolites. Geochimica et Cosmochimica Acta, 33, 247–255.

Bindeman, I.N. and Davis, A.M. (2000) Trace element partitioning between plagioclase and melt: Investigation of dopant influence on partition behavior. Geochimica et Cosmochimica Acta, 64, 2863–2878.

Bindeman, I.N., Davis, A.M., and Drake, M.J. (1998) Ion microprobe study of plagioclase-basalt partition experiments at natural concentration level of trace elements. Geochimica et Cosmochimica Acta, 62, 1175–1193.

Blundy, J.D. and Wood, B.J. (1991) Crystal-chemical controls on the partitioning of Sr and Ba between plagioclase feldspar, silicate melts, and hydrothermal solutions. Geochimica et Cosmochimica Acta, 55, 193–209.

Brice, J.C. (1975) Some thermodynamic aspects of the growth of strained crystals. Journal of Crystal Growth, 28, 249–253.

Christiansen, E.H., Bikun, J.V., Sheridan, M.F., and Burt, D.M. (1984) Geochemical evolution of topaz rhyolite from the Thomas Range and Spor Mountain, Utah. American Mineralogist, 69, 223–236.

Crisci, G.M., De Rosa, R., Esperanca, S., Mazzuoli, R., and Sonnino, M. (1991) Temporal evolution of a three component system: the island of Lipari (Aeolian Arc, southern Italy). Bulletin of Volcanology, 53, 207–221.

Donnelly-Nolan, J.M., Hearn, Jr.B.C., Curtis, G.H., and Drake, R.E. (1981) Geochronology and evolution of the Clear Lake Volcanics. United States Geological Survey Professional Paper, 1141, 47–60.

Drake, M.J. (1972) The distribution of major and trace elements between plagioclase feldspar and magmatic silicate liquid: an experimental study, 190 p. Dissertation, University of Oregon.

Drake, M.J. and Holloway, J.R. (1978) "Henry's law" behaviour of Sm in a natural plagioclase/melt system: importance of experimental procedure. Geochimica et Cosmochimica Acta, 42, 679–683.

Drake, M.J. and Weill, D.F. (1975) Partition of Sr, Ba, Ca, Y, Eu2 + , and other REE between plagioclase feldspar and magmatic liquid: An experimental study. Geochimica et Cosmochimica Acta, 39, 689–712.

Dudas, M.J., Schmitt, R.A., and Harward, M.E. (1971) Trace element partitioning between volcanic plagioclase and dacitic pyroclastic matrix. Earth and Planetary Science Letters, 11, 440–446.

Duffield, W.A. and Dalrymple, G.B. (1990) The Taylor Creek Rhyolite of New Mexico: A rapidly emplaced field of lava domes and flows. Bulletin of Volcanology, 52, 475–487.

Elkins, L.T. and Grove, T.L. (1990) Ternary feldspar experiments and thermodynamic models. American Mineralogist, 75, 544–559.

Ewart, A. and Taylor, S.R. (1969) Trace element geochemistry of the rhyolitic volcanic rocks, Central North Island, New Zealand, phenocryst data. Contributions to Mineralogy and Petrology, 22, 127–146.

Green, T.H. and Pearson, N.J. (1983) Effect of pressure on the rare earth element partition coefficients in common magmas. Nature, 305, 414–416.

Greenland, L.P. (1970) An equation for trace element distribution during magmatic crystallization. American Mineralogist, 55, 455–465.

Guo, J. and Green, T.H. (1989) Barium partitioning between alkali feldspar and silicate liquid at high temperature and pressure. Contributions to Mineralogy and Petrology, 102, 328–335.

Higuchi, H. and Nagasawa, H. (1969) Partition of trace elements between rock-forming minerals and the host volcanic rocks. Earth and Planetary Science Letters, 7, 281–287.

Hildreth, W. (1977) The magma chamber of the Bishop tuff: Gradients in temperature, pressure, and composition, 328 p. Ph.D. dissertation, University of California, Berkeley.

Holt, G. (1998) Trace element partitioning of alkali feldspar in Burro Mesa Rhyolite and other units of the Trans-Pecos magmatic province, 190 p. M.S. thesis, Baylor University, Waco.

Icenhower, J. and London, D. (1996) Experimental partitioning of Rb, Cs, Sr, and Ba between alkali feldspar and peraluminous melt. American Mineralogist, 81, 719–734.

Korringa, M.K. and Noble, D.C. (1971) Distribution of Sr and Ba between natural feldspar and igneous melt. Earth and Planetary Science Letters, 11, 147–151.

Lambert, R.S.J. and Holland, J.G. (1974) Yttrium geochemistry applied to petrogenesis utilizing calcium-yttrium relationships in minerals and rocks. Geochimica et Cosmochimica Acta, 38, 1393–1414.

Le Bas, M.J., Le Maitre, R.W., Streckeisen, A., and Zanettin, B. (1986) A chemical classification of volcanic rocks based on the total alkali-silica diagram. Journal of Petrology, 27, 745–750.

Leeman, W.P. and Phelps, D.W. (1981) Partitioning of rare earth and other trace elements between sanidine and coexisting volcanic glass. Journal of Geophysical Research, 86, 10193–10199.

Lindsey, D.A. (1982) Tertiary volcanic rocks and uranium in the Thomas Range and northern Drum Mountains, Juab County, Utah. 71 p. United States Geological Survey Professional Paper, 1221.

MacLeod, N.S., Walker, G.W., and McKee, E.H. (1976) Geothermal significance of eastward increase in age of upper Cenozoic rhyolitic domes in southeastern Oregon. In Proceedings, Second United Nation Symposium on the Development and Use of Geothermal Resource, 1, 465–474.

Mahood, G.A. and Hildreth, W. (1983) Large partition coefficients for trace elements in high-silica rhyolite. Geochimica et Cosmochimica Acta, 47, 11–30.

Masuda, A. and Kushiro, I. (1970) Experimental determinations of partition coefficients of ten rare earth elements and barium between clinopyroxene and liquid in the synthetic system of 20 kilobar pressure. Contributions to Mineralogy and Petrology, 26, 42–49.

Miller, C.D. (1985) Holocene eruptions at the Inyo volcanic chain, California: implications for possible eruptions in Long Valley. Geology, 13, 14–17.

Mysen, B.O. (1976) Rare earth partitioning between crystals and liquid in the upper mantle. Carnegie Institution Washington, Yearbook, 75, 656–659.

——— (1978) Limits of solution of trace elements in mineral according to Henry's law: review of experimental data. Geochimica et Cosmochimica Acta, 42, 871–885.

Nagasawa, H. and Schnetzler, C.C. (1971) Partitioning of rare earth, alkali and alkaline earth elements between phenocrysts and acidic igneous magma. Geochimica et Cosmochimica Acta, 35, 953–968.

Nash, W.P. and Crecraft, H.R. (1985) Partition coefficients for trace elements in silicic magmas. Geochimica et Cosmochimica Acta, 49, 2309–2322.

Nelson, C.H., Bacon, C.R., Robinson, S.W., Adam, D.P., Bradbury, J.P., Barber, J.H. Jr., Schwartz, D., and Vagenas, G. (1994) The volcanic, sedimentologic, and paleolimnologic history of the Crater Lake caldera floor, Oregon: Evidence for small caldera evolution. Geological Society of America Bulletin, 106, 684–704.

Philpotts, J.A. and Schnetzler, C.C. (1970) Phenocryst-matrix partition coefficients for K, Rb, Sr, and Ba, with applications to anorthosite and basalt genesis. Geochimica et Cosmochimica Acta, 34, 307–322.

Price, J.D. (1993) The nature and origin of the intermediate and silicic rocks, and their mafic inclusions, at South Sister volcano, central high Cascades, 169 p. MS thesis, Baylor University, Waco, Texas.

Ragland, P.C. (1989) Basic analytical petrology, 369 p. Oxford University Press, Oxford, New York.

Ren, M. (1997) Composition variation within and eruption dynamics of the El Cajete Series, Valles Caldera, New Mexico, 220 p. MS thesis, Baylor University, Waco, Texas.

Ren, M., Parker, D.F., and White, J.C. (2000) Systematic control of crystal and melt chemistry on feldspar trace element partitioning for Rb, Sr, and Ba, Part II: metaluminous and peraluminous rhyolite. Geological Society of America Abstracts with Programs, 32, 147–148.

Rinehart, C.D. and Huber, N.K. (1965) The Inyo Crater Lakes—a blast in past: California Division of Mines and Geology, Mineral Information Service, 18, 169–172.

Sampson, D.E. and Cameron, K.L. (1987) The geochemistry of the Inyo volcanic chain: Multiple magma systems in the Long Valley region, eastern California. Journal of Geophysical Research, 92, 10403–10421.

Schnetzler, C.C. and Philpotts, J.A. (1970) Phenocryst matrix partition coefficients of rare-earth elements and barium between igneous matrix material and rock forming mineral phenocrysts I. In Ahrens. L.H. Ed., Origin and distribution of the elements, Pergamon, 929–938.

Scott, W.E. (1983) Character and age of Holocene rhyodacite eruptions at South Sister Volcano, Oregon. EOS Transactions, American Geophysical Union, 64, 899–900.

——— (1987) Holocene rhyolite eruptions on the flanks of South Sister volcano, Oregon. In Fink, J.H., Ed. Geological Society of America Special Paper 212, 35–53.

Self, S., Goff, F., Gardner J.N., Wright, J.V., and Kite, W.M. (1986) Explosive rhyolite volcanism in the Jemez mountains: Vent locations, caldera development and relation to regional structure. Journal of Geophysical Research, 91, 1779–1798.

Self, S., Kircher, D.E., and Wolff, J.A. (1988) The El Cajete Series, Valles Caldera, New Mexico. Journal of Geophysical Research, 93, 6113–6127.

Shannon, R.D. (1976) Revised effective ionic radii in oxides and fluorides. Acta Crystallographica, A32, 751–757.

Shimizu, N. (1978) Analysis of zoned plagioclase of different magmatic environments: a preliminary ion-microprobe study. Earth and Planetary Science Letters, 39, 398–400.

Sieh, K. and Bursik, M.I. (1986) Most recent eruption of the Mono Craters, eastern central California. Journal of Geophysical Research, 91, 12539–12571.

Simon, S.D., Kuehher, S.M., Davis, A.M., Grossman, L., Johnson, M.L., and Burnett, D.S. (1994) Experimental studies of trace element partitioning in Ca, Al-rich compositions: anorthite and perovskite. Geochimica et Cosmochimica Acta, 58, 1507–1523 (S2).

Spell, T.L. and Kyle, P.R. (1989) Petrogenesis of Valle Grande Member rhyolites, Valles Caldera, New Mexico: Implications for evolution of the Jemez Mountains magmatic system. Journal of Geophysical Research, 94, 10379–10396.

Spell, T.L., Kyle, P.R., Thirlwall, M.F., and Campbell, A.R. (1993) Isotopic and geochemical constraints on the origin and evolution of postcollapse rhyolites in the Valles Caldera, New Mexico. Journal of Geophysical Research, 98, 19732–19739.

Stimac, J.A., Pearce, T.H., Donnelly-Nolan, J.M., and Hearn, Jr. B.C. (1990) The origin and implications of undercooled andesitic inclusions in rhyolites, Clear Lake Volcanics, California. Journal of Geophysical Research, 95, 17729–17746.

Sun, C., Williams, R.J., and Sun, S. (1974) Distribution coefficients of Eu and Sr for plagioclase-liquid and clinopyroxene-liquid equilibria in oceanic ridge basalt: an experimental study. Geochimica et Cosmochimica Acta, 38, 1415–1433.

Toyoda, S., Goff, F., Ikeda, S., and Ikeya, M. (1995) ESR dating of quartz phenocrysts in the El Cajete and Battleship Rock Members of Valles Rhyolite, Valles Caldera, New Mexico. Journal of Volcanology and Geothermal Research, 67, 29–40.

Tuttle, O.F. and Bowen, N. L., (1958) Origin of granite in the light of experimental studies in the system $NaAlSi_3O_8$-$KAlSi_3O_8$-SiO_2-H_2O, 153 p. Geological Society of America, Memoir 74.

Wen, S.(1996) The program SOLVCALC 2, http:\\sbmp96.ess.sunysb.edu\SolvCalc. Upgrade program based on Wen, S. and Nekvail, H. (1994) SOLVCALC: An interactive graphics program package for calculating the ternary feldspar solvus and for two-feldspar geothermometry: Computers and Geosciences, 20, 1025–1040.)

White, J.C. (2003) Trace-element partitioning between alkali feldspar and peralkalic quartz trachyte to rhyolite magma. Part II: Empirical equations for calculating trace-element partition coefficients of large-ion lithophile, high field-strength, and rare-earth elements. American Mineralogist, 88, 330–337.

White, J.C., Parker, D.F., and Ren, M. (2000) Systematic control of crystal and melt chemistry on feldspar trace element partitioning for Rb, Sr, and Ba, Part I: peralkalic trachyte and rhyolite. Geological Society of America Abstracts with Programs, 32, 148.

Wilson, M. (1989) Igneous petrogenesis: a global tectonic approach, 466 p. Unwin Hyman, London.

Wood, S.H. (1977) Distribution, correlation, and radiocarbon dating of late Holocene tephra, Mono and Inyo craters, eastern California. Geological Society of America Bulletin, 88, 89–95.

Wood, B.J. and Fraser, D.G. (1976) Elementary thermodynamics for geologists, 303 p. Oxford University Press.

MANUSCRIPT RECEIVED SEPTEMBER 27, 2002
MANUSCRIPT ACCEPTED MARCH 18, 2003
MANUSCRIPT HANDLED BY JOHN AYERS